Journal of Materials Science: Materials in Electronics (2018) 29:7345–7355
https://doi.org/10.1007/s10854-018-8724-x

Photoreduction *of 4-Nitrophenol* in the presence of carboxylic acid using CdS nanofibers

Agileo Hernández-Gordillo[1] · Próspero Acevedo-Peña[2] · Monserrat Bizarro[1] · Sandra E. Rodil[1] · Ricardo Gómez[3]

Received: 6 November 2017 / Accepted: 1 February 2018 / Published online: 7 February 2018

Abstract
The photocatalytic reduction of *4-Nitrophenol* was assisted with blue light irradiation using CdS semiconductor nanofiber. The kinetic study of the blue-photoreduction of *4-Nitrophenol* to *4-Aminophenol* was performed by using Na_2SO_3 as "hole scavenger" in the presence of middle carboxylic acids (acetic, oxalic and citric acid). The effect of photocatalyst load, the carboxylic acid concentration and of the pH solution (acid, neutral and alkaline media) were investigated. The maximum *4-Nitrophenol* photoreduction rate was reached in neutral media and it is related to the enhanced "hole scavenging" effect caused by the SO_3^{2-} or HSO_3^{2-} ions in the presence of carboxylic acid. Electrochemical characterization of CdS nanofiber was made in the presence of 4-*NP* and citric acid. The *4-NP* photoreduction reaction follows a zero order reaction and a possible mechanism to explain the fast electron transfer process is discussed as a consequence of the carboxylic acid adsorbed on the CdS surface.

1 Introduction

Aminophenols are an important class of organic compounds used as secondary intermediates in the manufacture of dyes, agrochemicals, analgesic, antipyretic drugs and pharmaceuticals substances such as paracetamol [1, 2]. Several methods exist for the preparation of aminophenols, including the reduction of the nitroaromatic compounds, which are well known as the most common contaminants present in industrial and agricultural which are discharge in wastewaters that provoke important damages to the environment because induce serious toxicological threat to ecosystems and human health [3]. From the environmental and economic point of view, an efficient approach for cleaner and cheap reduction of aminoaromatic compounds is still under investigation about organic synthesis [4–6].

Nowadays, an attractive alternative for the organic chemical transformation of *4-nitrophenol* (*4-NP*) to *4-aminophenol* (*4-AP*) is the photoassisted reduction reaction using semiconductor nanomaterials under visible light irradiation at room temperature (soft condition) [1, 4, 7]. Typically, the photoassisted chemical reduction reaction requires the use of an adequate reactant molecule called "hole scavenger" for the holes consumption, which avoids the recombination of the photogenerated electron–hole pairs, allowing the electron transfer process and increasing the efficiency of the photoassisted reduction reaction [1, 7–9]. For the nitroaromatic photoreduction using semiconductors like metal oxides, metal sulfides or mixtures of them, the commonly used "hole scavengers" are the alcohols (methanol, ethanol, isopropanol) [4, 7, 10–13], ammonium oxalate or formate ($NH_4C_2O_2$, NH_4HCO_2) [8, 14–16] and sodium sulfite (Na_2SO_3) [14, 17–21]. In few cases, organic carboxylic acids (like oxalic or formic) can also act as "hole scavengers", because they react with the *holes* to produce active $\bullet CO_2^-$ radicals, which have strong reductive ability ($\bullet CO_2^-/CO_2$, − 1.8 V vs. NHE) and can reduce nitroaromatics compounds [8, 22, 23].

Most of these studies have demonstrated that among the metal sulfide semiconductors, the CdS is an efficient

Agileo HernándezGordillo and Próspero AcevedoPeña: CONACYT Research Fellow.

✉ Agileo Hernández-Gordillo
agileo12@hotmail.com; agileohg@iim.unam.mx

[1] Instituto de Investigaciones en Materiales, Universidad Nacional Autónoma de México, Circuito Exterior SN, Ciudad Universitaria, 04510 Coyoacán, Mexico City, Mexico

[2] Conacyt-Centro de Investigación en Ciencia Aplicada y Tecnología Avanzada-Unidad Legaria, IPN, 11500 Mexico City, Mexico

[3] Depto. de Química, Área de Catálisis, Grupo ECOCATAL, Universidad Autónoma Metropolitana-Iztapalapa, Av. San Rafael Atlixco No 186, Mexico City 09340, Mexico

light-induced photocatalysts [14, 24–29], because of its blue-photogenerated electrons exhibit stronger reductive ability and can participate in the reduction reaction by the electron-transfer process. Nevertheless, its efficiency depends on the "hole scavenger" type used for the *holes* consumption, or on its concentration and the reaction conditions [14, 17]. By using Na_2SO_3 as "hole scavenger", the photogenerated *holes* react with sulfite (SO_3^{2-}) ions forming sulfite ($\bullet SO_3^-$) radical with the subsequent transformation toward sulfate (SO_4^{2-}) ions and dithionate ($S_2O_6^{2-}$) ions, which both could be adsorbed on the semiconductor surface limiting the photocatalytic efficiency. However, the elimination of these oxysulfur species might be possible using carboxylic acid (ROOH or ROO–), because under irradiation conditions, it reacts with the formed sulfur ($\bullet SO_4^-$ or $\bullet SO_3^-$) radicals, acting as "radical scavenger" [30, 31].

As far as we know, photoreduction of *4-NP* to *4-AP* using Na_2SO_3 in combination with organic carboxylic acids as either "hole scavenger" or as "radical scavenger" has not been applied. With this in mind, the photoreduction of *4-NP* to *4-AP* under blue light irradiation using CdS nanofibers in the presence of either Na_2SO_3 or middle carboxylic acid or combination of both (Na_2SO_3 and carboxylic acid) was investigated. The effect of CdS photocatalyst load, the influence of type and contents of carboxylic acids (citric acid, oxalic acid and acetic acid) and the solution pH were explored. The impact of the presence of carboxilic acids on the kinetics of *4-NP* photoreduction as well as the interaction between Na_2SO_3, carboxylic acid and the CdS surface were discussed using conventional photocatalytic studies combined with (photo)electrochemical characterization. The use of middle carboxylic acids as either "hole scavenger" or as "radical scavenger" was discussed.

2 Experimental section

2.1 Synthesis of the CdS nanofibers

The CdS nanofibers were synthesized by a precipitation method in a mixture of solvent of H_2O:ethylenediamine(*EN*):tetrahydrofuran(THF) (10:60:30 vol%) at moderate synthesis conditions [32]. Appropriate amounts of $Cd(NO_3)_2H_2O$ (Reasol) were dissolved in THF–H_2O solution at room temperature with constant stirring and then the *EN*-solvent was added. After, carbon disulfide (CS_2) was added drop wise, maintaining a stoichiometry molar ratio of S:Cd of 1:1, then the transparent mixture solution was heated at boiling point (~ 70–80 °C) under vigorous magnetic stirring for 2 h and subsequently cooled at room temperature. Finally, the resulting yellow precipitate was collected by filtration, washed with ethanol–water solution and dried at 80 °C for 1 h.

2.2 Characterization of semiconductor

The CdS photocatalyst was characterized by X-ray powder diffraction using an X-ray diffractometer Siemens D500 with Cu $K\alpha$ radiation (50 kV, 40 mA). The scanning rate was 0.03 °/S in the 2θ range from 5° to 70°. The band-gap energy was calculated using the Kubelka–Munk method from the diffuse reflectance spectra obtained with a Varian Cary-100 spectrometer equipped with an integration sphere. The morphology and the microstructural parameter was determined by High Resolution Transmission Electron Microscope (HRTTEM) JEOL ARM-200F microscope, equipped with a field emission gun, operating at 200 kV.

2.3 Blue-photoreduction of *4-Nitrophenol* (*4-NP*)

The photocatalytic reaction was carried out in a glass home-made reactor system containing 200 mL of an aqueous solution with 30 ppm of *4-NP* (Aldrich) and 200 mg (8 mM) of Na_2SO_3 as "hole scavenger" [17]. The photocatalysts load powder ranged from 0.025 to 0.15 mg/L and the carboxylic acid contents ranged from 1 to 16 mM. The desired pH solution 4, 6 or 9 was adjusted with a drop of concentrated H_2SO_4 or NH_4OH. Once the optimal photocatalyst load (10 mg) of the CdS, solution pH, Na_2SO_3 and citric acid contents were established, additional photoreduction experiments were performed in order to determine its recyclability. Therefore, four cycle experiments with the same CdS nanofibers, recovered by decantation, was used again for 40 min. In all cases, the suspension was maintained by magnetic stirring (600 rpm) in the absence of bubbled air at room temperature and was left under dark conditions for 30 min to ensure the adsorption–desorption equilibrium. Subsequently, the suspension was irradiated with blue light supplied by a blue LED Lamp emitting at $\lambda = 450$ nm of low luminous fluxes (190 Lumens) and low power (3 W), located at ~ 7 cm from the suspension. The estimation of the concentration of photoreduced *4-NP* was made by UV–Vis spectroscopy using a Varian-Cary 100 spectrometer, by following the disappearance at 315 nm in acid media, 400 nm in alkaline media or by the isosbestic point at 345 nm in either acid or alkaline media. The kinetic data such as the apparent rate constant (K_{app}) in the photoreduction reactions were obtained considering a pseudo zero order reaction. The Langmuir–Hinshelwood kinetic model is usually applicable to describe the kinetics of *4-NP* reduction on photocatalyst like CdS [17].

2.4 Electrochemical characterization

To characterize the effect of Na_2SO_3 (8 mM) and $C_2H_4O_2$ (4 mM) over the semiconducting properties and photoelectrochemical behavior of CdS nanofibers here synthesized, CdS films were supported over ITO by drop casting as follows: ITO substrates were cleaned in an ultrasonic bath using acetone and milliQ water, after that a squared area of 0.25 cm^2 was delimited and 25 µL of a 0.1 g/L CdS suspension in ethanol was dropped over the substrate. The films were left to dry at room temperature, and finally were heated at 80 °C to eliminate the remnant ethanol. It is worth mentioning that a higher temperature was prohibited since it could induce irreversible structural changes in the CdS nanoparticles [32]. The electrochemical characterization were performed in a conventional three-electrode cell using $Hg/Hg_2SO_4/K_2SO_4$ (sat) as reference electrode (E_{ref} = 0.64 V vs. NHE), a graphite bar (99.995% of purity) as counter electrode and the former prepared CdS/ITO films as working electrode. As supporting electrolyte was employed a 30 mM $KClO_4$ solution in MilliQ water. The (photo)electrochemical characterization of CdS supported on ITO was performed under three different scenarios: *(i)* in presence of a electrolyte 30 mM $KClO_4$ in water (labeled as support), *(ii)* in presence of a electrolyte 30 mM $KClO_4$/8 mM Na_2SO_3 in water (labeled as sulfite) and, *(iii)* in presence of a electrolyte 30 mM $KClO_4$/8 mM Na_2SO_3/4 mM $C_6H_8O_7$ in water (labeled as sulfite + citric). In all cases the solution pH was fixed to a value of 9.0 using NaOH. Furthermore, the solutions employed for the (photo)electrochemical tests were previously bubbled with N_2 gas during 15 min to displace the dissolved oxygen. All the experiments were carried out in a Potentiostat/Galvanostat CH Instruments model CHI-604E and a blue-LED lamp of 3W was also used.

3 Results and discussion

3.1 Characterization of CdS semiconductor

The morphology of the CdS sample was as flexible fibers-like (Fig. 1a) with diameter (*D*) ranging from 4 to 25 nm and a length (*L*), difficult to determine, but probably varying between 100 and 500 nm. The specific surface area of the CdS nanofibers is 152 m^2/g. The X-ray diffraction pattern of the CdS nanofibers shows reflection peaks of the (*100*), (*002*) and (*101*) planes (Fig. 1b) corresponding to the hexagonal phase (JCPDS No. 41-1049), with lattice parameter ($a = 0.415$ nm and $c = 0.66$ nm) close to the values reported for the bulk CdS. The average nanocrystallite size from the diffraction peak of the (002) plane is around 8 nm. CdS nanofibers exhibit absorption edge in the visible light region close to 460–490 nm attributed to the intrinsic band-gap transition of electron from the valence band to the conduction band. The shaded area in the Fig. 1c, corresponds to the emission spectrum of the blue LED lamp used for the CdS activation. The band-gap energy is 2.6 eV, which was slightly blue-shifted probably by the presence of sulfur vacancies. These vacancies are generated because of the *EN*-solvent is linked on the superficial Cd^{2+} ions of the nanofibers, creating surface states that act as electron-traps, prolonging the lifetime of the photogenerated electrons and promoting the electron–hole separation [32].

3.2 Blue-photoreduction of *4-Nitrophenol*

When the *4-Nitrophenol (4-NP)* solution contains Na_2SO_3 (8 mM) and the pH of the solution is alkaline (pH = 9), two absorption bands were observed at 210 and 400 nm (Fig. 2a). These bands correspond to the sulfite (SO_3^{2-}) ions and *4-nitrophenolate (4-NPhate)* ions formation, respectively [17, 18]; however, these bands were modified by the addition of organic carboxylic acid due to the generated acid condition. So the absorption band at 400 nm of *4-NPhate* ion decreased while the absorption band at 315 nm of *4-NP (neutral specie)* increased as the initial pH solution

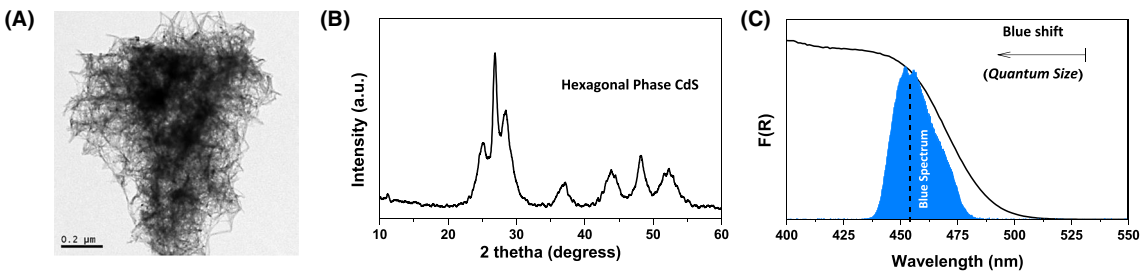

Fig. 1 **a** TEM image, **b** X-ray diffraction pattern and **c** UV–Vis DRS of CdS nanofibers

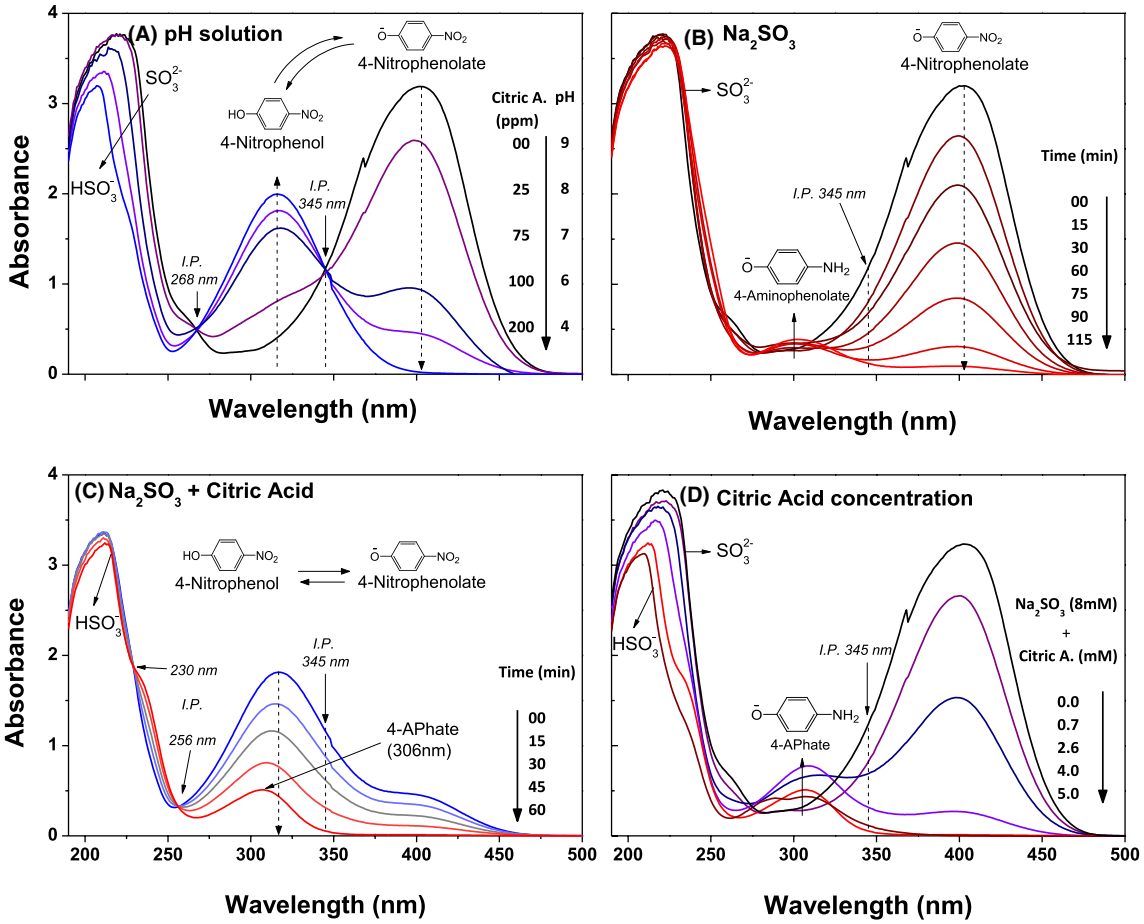

Fig. 2 Absorbance spectra of: **a** *4-NP* solution containing Na_2SO_3 (8 mM) as a function of the solution pH modified by the addition of citric acid (0–5 mM); photoreduction of *4-NP* containing **b** Na_2SO_3 (pH 9) and **c** Na_2SO_3 and citric acid (pH 6); **d** *4-APhate* ion formation as function of the citric acid concentrations at 60 min by using CdS (0.5 g/L)

decreased from 9 to 4, which was caused by the increasing of the citric acid concentration. The change of equilibrium species of *4-NPhate* ion toward to *4-NP* species formation was influenced by the solution pH [33, 34]. For this reason, the *4-NP* concentration was determined from the isosbestic points (I.P.) at either 268 or 345 nm, because its molar absorptivity at these wavelengths does not change by effect of the pH [35]. On the other hand, the absorption band of SO_3^{2-} ions (210 nm) is blue-shifted by the decrease of the pH caused by the citric acid addition, indicating that the equilibrium of SO_3^{2-} ions was displaced into the formation of HSO_3^- species [36, 37]. During the blue-photoreduction of *4-NPhate* ion containing SO_3^{2-} ions by using CdS nanofibers (Fig. 2b), the absorption band of the SO_3^{2-} ions was unaltered and the absorption band of *4-NPhate* ions decreased while the absorption band at 300 nm increased due to the *4-aminophenolate (4-APhate)* ion formation as the time progressed [33, 38]. In the same manner, when the blue-photoreduction of *4-NP* and *4-NPhate* species in equilibrium was conducted with HSO_3^- ions and citric acid (Fig. 2c), the absorption band of the HSO_3^{2-} ions was also unchanged. Besides, the absorption band of both anionic and neutral *4-NP* species decreased as the time progressed until the appearance of the band of *4-APhate* ion formation [33]. In addition, the isosbestic point at 230 and 256 nm indicates equilibrium between the reactant and the product, suggesting that secondary products are not formed.

The absorbance spectrum of the photoreduction of *4-NP* varies depending on the citric acid concentrations, however, in all cases the band associated to the *4-APhate* ion formation was observed (Fig. 2d) and the relative concentration (C/C_0) of *4-NP* was determined from the isosbestic point at 345 nm.

3.3 Effect of the photocatalyst load and pH using Na_2SO_3

The C/C_0 of *4-NP* during the photoreduction of *4-NP* containing Na_2SO_3 using CdS nanofibers, yielded a straight line, which suggested that the kinetic rate is adjusted to a

zero order reaction (not shown). This zero order kinetic is observed when the disappearance rate of the *4-NP* reactant is constant as the time progresses, indicating that the photoreduction rate is independent of *4-NP* reactant concentration. The zero order kinetic rate constant is typically obtained when the optical density of the reaction solution is large due to the relatively high concentrations of reactant and of photocatalyst, leading to the completed absorption of the incident blue light. Therefore a constant decrease of the reactant and a constant formation of the products during the course of the reaction are achieved [29]. The *4-NP* photoreduction containing Na_2SO_3 without photocatalyst was negligible (not shown), indicating that the CdS nanofibers are needed as photocatalysts to conduct the photoassisted reduction reaction.

The amount of CdS photocatalyst was varied in the interval of 0.025–0.15 g/L to ensure the optimal value for the photoreduction of 30 ppm of *4-NP* with the addition of 8 mM of Na_2SO_3 (pH 9). The kinetic rate vs photocatalyst load plot exhibited two segments (Fig. 3a); the first one at photocatalyst loads < 0.1 g/L showed a linear relationship with the photocatalyst load; but at loads higher than 0.1 g/L, the kinetic rate presented a plateau (second segment). This plateau region is related to a narrowing of the region in which the photocatalytic reaction occurs, generated by the absorption and scattered light caused by the photocatalyst particles. In order to ensure an efficient absorption of photons in our reaction system and that the photocatalytic reaction is not influenced by the scattered light, we chose a photocatalyst load of 0.05 g/L.

The influence of the solution pH on the photocatalytic properties of CdS nanofibers for the photoreduction reaction of *4-NP* was also investigated. For this, the pH of the solution containing *4-NP* and Na_2SO_3 was varied from 4 to 9 using either H_2SO_4 or NaOH, finding that the kinetic rate constants were slightly modified, obtaining a maximum at neutral conditions (pH 6.2, Fig. 3b). Considering that in alkaline media the species are *4-NPhate* and SO_3^{2-} ions, while in acid media are *4-NP* and HSO_3^- ions, the similar kinetic rate values obtained at this two pHs suggests that the photoreaction does not depend on the solution pH and neither on the different sulfur species formed. This is expected to occur since it has been demonstrated that the adsorption of *4-NP* or *4-NPhate* ion on CdS surfaces can occur via the nitrogroup (–NO_2) [38] and the photodecomposition of either SO_3^{2-} or HSO_3^- ions occur in the same way, acting as "hole scavengers" that lead to the formation of $\bullet SO_3^-$ radicals, achieving the electron transfer process [39].

3.4 Effect of the citric acid (solution pH and concentrations)

The C/C_0 of *4-NP* during its photoreduction containing Na_2SO_3 in the presence of citric acid (4 mM) by using 0.05 g/L of CdS nanofibers at pH ~ 6.2, also yielded a straight line which suggested that the kinetic rate is also adjusted to a zero order reaction. The photoreaction of *4-NP* containing citric acid in absence of Na_2SO_3 was also negligible, indicating that the citric acid alone cannot act as "hole scavenger" and that Na_2SO_3 is needed to conduct the blue-photoassisted reduction reaction. The kinetic curve of *4-NP* photoreduction containing Na_2SO_3 is faster in presence of citric acid than that in absence of it, indicating that the *4-NP* photoreduction is greatly improved with the carboxylic acid addition.

When citric acid (4 mM) was used to improve the *4-NP* photoreduction containing either SO_3^{2-} or HSO_3^- ions, the kinetic curve plot was also slightly changed when the solution pH was modified, obtaining the maximum kinetic rate constant at the same pH conditions (pH ~ 6.2, Fig. 4a). It is known that depending on the solution pH in dark conditions, different sulfur species in presence of carboxylic acid should be formed [39]. In alkaline media, the SO_3^{2-} ions act as good S-nucleophiles, which attack one of the two oxygen atoms in the carboxylic acid (RCOOH), without any intermediate formation. On the contrary, at pH 4.5, the citric acid is in the ionic form ($RCOO^-$) and it reacts with the HSO_3^- ion through the formation of at least two

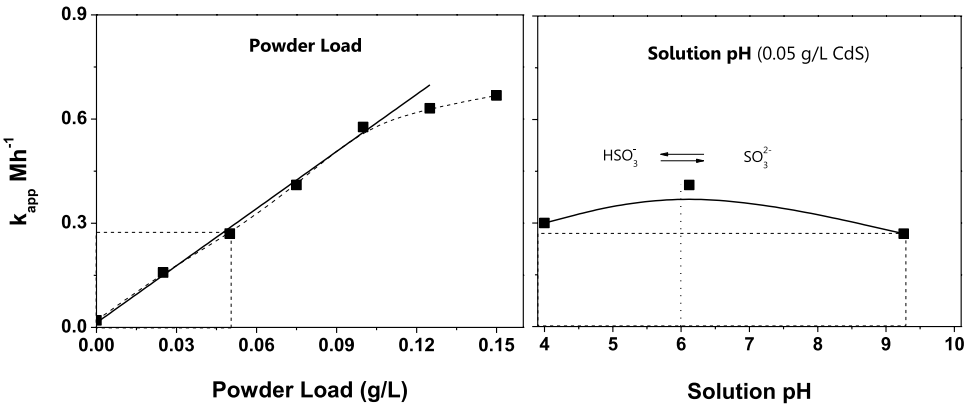

Fig. 3 Plot of the apparent kinetic rate constant of *4-NP* photoreduction in presence of Na_2SO_3 as function of: **a** CdS powder load at pH 9.3; and **b** Solution pH using CdS (0.05 g/L)

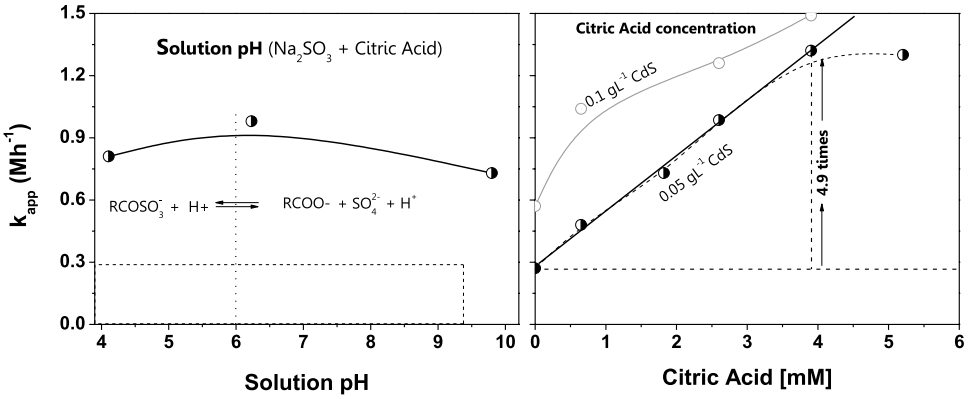

Fig. 4 Plot of the apparent kinetic rate constant of *4-NP* photoreduction in presence of citric acid (2.6 mM, pH 6) and Na_2SO_3 as function of: **a** solution pH using CdS (0.05 g/L); and **b** citric acid concentration at 0.05 and 0.1 g/L of CdS

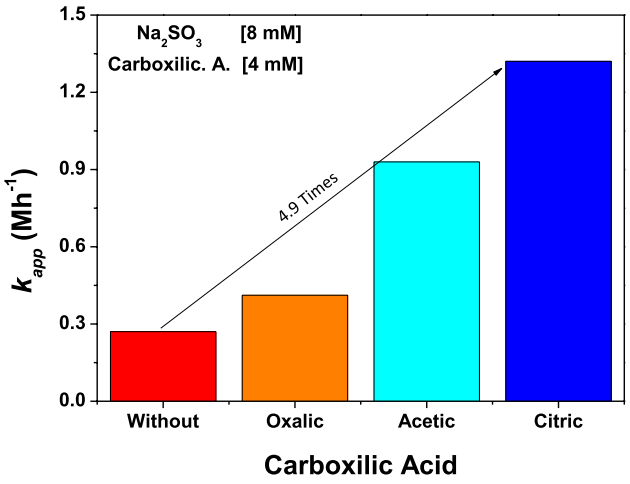

Fig. 5 Apparent kinetic rate constant for the *4-NP* photoreduction using different middle carboxylic acid at 4 mM

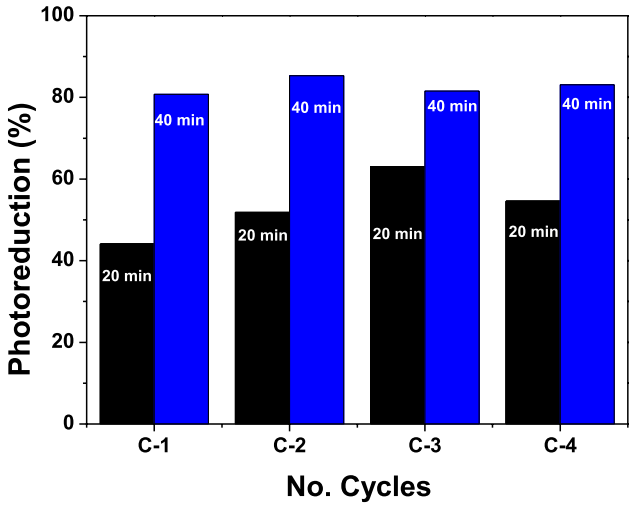

Fig. 6 Recyclability of CdS nanofibers for the *4-NP* photoreduction in the presence of Na_2SO_3 and citric acid for four cycles

intermediates, $RCOOSO_2^-$ or $RCOOSO_2H$ and $RCOSO_3^-$. However, under irradiation conditions, the carboxylic acid could react with the formed sulfur radicals ($\bullet SO_3^-$), suggesting that it could play role as "radical scavenger" [30, 31].

In order to study the influence of the concentrations of citric acid in the *4-NP* photoreduction containing Na_2SO_3 (8 mM), the citric acid concentration was varied in the interval of 0.7 to 5 mM and the apparent reaction rate constants were estimated for each concentration (Fig. 4b). The obtained curve plot exhibited two segments; the first one at concentrations < 4 mM showed a linear relationship of the apparent kinetic rate constant with the citric acid concentration. Meanwhile, at concentrations higher than 4 mM, the kinetic rate presented a plateau (second segment), suggesting that the *4-NP* photoreduction does not depend on the citric acid concentration. This plateau region is similar to the one that occurs when the photocatalyst load is varied and it might be generated by the adsorption of the citric acid on the whole surface of the photocatalyst particles. The CdS surface is prone to be modified by the citric acid because it can be linked to the superficial Cd^{2+} of the CdS semiconductor [40], allowing to enhance the "hole scavenging" effect and the fast electron transfer process.

For comparison, other middle organic carboxylic acids were also tested (Fig. 5). The photocatalytic reaction by using either acetic acid or oxalic acid in the absence of either SO_3^{2-} or HSO_3^- ions was also negligible (not shown), indicating that any carboxylic acid alone cannot act as "hole scavenger" using CdS photocatalyst. The "hole consumption" process on the CdS surface caused by adsorption of either SO_3^{2-} or HSO_3^- ions was not affected by oxalic acid addition, suggesting probably that the oxalic acid does not interact with the CdS surface. The kinetic rate constants, obtained with the different carboxylic acids at the same concentration (4 mM), was 1.5 times larger with oxalic acid than without it, ~ 3 times larger with acetic acid and ~ 5 times larger with citric acid (Fig. 5).

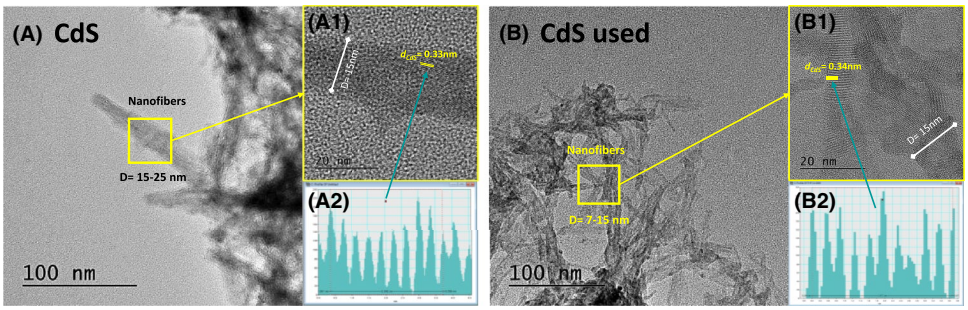

Fig. 7 HRTEM image and lattice fringes calculated for: **a** CdS before the reaction and **b** CdS re-used after of 4th cycles of blue-reaction

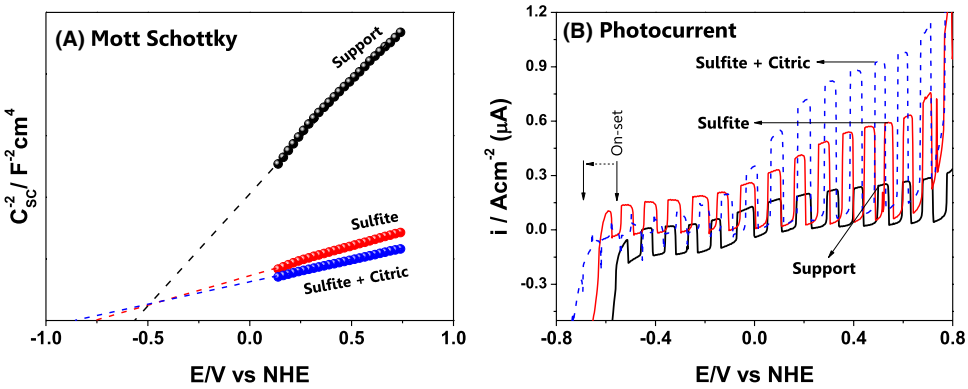

Fig. 8 **a** Plot the C_{SC}^{-2} versus potential curves and **b** plot of photocurrent versus potential using Blue-LED lamp, obtained for the CdS/ITO in the three different scenarios

3.5 Recyclability and stability of CdS nanofibers

It is known that CdS suffers photocorrosion phenomena during the photocatalytic process, but in the presence of Na_2SO_3 as sacrificial reagent, CdS is chemically stable as was previously demonstrated [17]. In order to demonstrate the recyclability of CdS nanofibers in presence of both Na_2SO_3 and citric acid, CdS was re-used for four cycles of reaction. The recyclability test revealed that the CdS nanofibers maintain their high activity of photoreduction (80–82%) for the four cycles of 40 min (Fig. 6). This indicates that CdS is resistant to the photocorrosion phenomena in the reaction media thanks to the presence of adequate hole scavengers, suggesting larger durability to carry out the photoreduction reaction.

The stability of the microstructure of the CdS nanofibers after of the photoreduction reaction was investigated by HRTEM. The HRTEM images of fresh CdS (Fig. 7a) and re-used CdS spent (Fig. 7b) showed diameter of nanofiber between 7 and 25 nm and that the regular lattice fringes of ca. 0.33–0.34 nm, corresponding to the (002) crystal planes of the hexagonal structure of CdS. It suggests that the CdS growth in the preferential c-axis [001] direction and that the stability of re-used CdS spent is well remained after the photocatalytic process.

3.6 Electrochemical characterization

The experimental data obtained until now indicate that sulfite (SO_3^{2-}) ions and citric acid have noteworthy impact over the photocatalytic reduction of *4-NP* at different pHs; however, the role played by these compounds during the photocatalytic process or on the CdS properties remains unclear. For this reason, (photo)electrochemical characterization of CdS nanofibers supported on ITO was performed under three different scenarios, in presence of: *(i)* supporting electrolyte (30 mM $KClO_4$), *(ii)* supporting electrolyte and Na_2SO_3 and, *(iii)* supporting electrolyte, Na_2SO_3 and $C_6H_8O_7$, as was described in the methodology. All the experiments were performed at a constant pH (~9) as this parameter influence the reduction potential of the electrons in CdS [41].

Table 1 Impact of the electrolyte composition over the semiconducting properties of CdS nanofibers

Electrolyte	E_{fb}/V versus NHE	$N_d/10^{20}\times cm^{-3}$
Support	−0.61	0.91
Sulfite	−0.76	3.31
Sulfite + citric	−0.82	4.24

The semiconducting properties of the CdS nanofibers under the three different scenarios were estimated from differential capacitance measurement at a constant frequency of 1 kHz, in a potential window in which no faradaic process are expected in the dark condition. The space charge capacitance was estimated from the imaginary component of the impedance measured [$-C_{SC}=(\omega Z_{img})^{-1}$]. The C_{SC}^{-2} versus potential curves obtained for the CdS/

ITO films in the three different scenarios are shown in Fig. 8a. In all cases a linear region with positive slope was observed, confirming that CdS is a n-type semiconductor. The flat band potential (E_{fb}) and the donor density (N_d) were estimated by fitting the Mott–Schottky equation for n-type semiconductors (Eq. 1), and are tabulated in Table 1.

$$\frac{1}{C_{sc}^2} = \frac{2N_A}{N_d F \varepsilon_r \varepsilon_0}\left[E_m - E_{fb} - \frac{RT}{F}\right] \quad (1)$$

where N_A is the Avogadro's number (6.02×10^{23} mol^{-1}), N_d is in cm^{-3}, F is the Faraday constant (~9.65×10^{4} C mol^{-1}), ε_r is the relative permittivity (assumed to be 8.9 for CdS [42]), ε_0 is the permittivity of vacuum (8.8542×10^{-14} F cm^{-1}), E_m (V) is the potential at which the measurement was carried out, E_{fb} is in V, R is the gas constant (8.314 J K^{-1} mol^{-1}), and T is the absolute temperature (~298 K). The third term in the parentheses can be assumed to be negligible compared to the remaining three terms at room temperature.

The E_{fb} (−0.61 V) of CdS/ITO in the presence of the electrolyte at pH ~9 is close to the reported value [43], but the addition of sulfite and sulfite + citric acid displaced the E_{fb} towards more negative potential values (Table 1), indicating that the electrons in CdS can present a more reductive potential in presence of these two compounds (−0.82 eV vs. NHE), which is favorable for *4-NP* photoreduction process (−0.3 eV vs. NHE at pH 9) [44]. Additionally, an increase in the N_d (Table 1) was also obtained, which indicates that adsorption of sulfite and citric acid on the CdS surface induces energetic states under its conduction band. These states might act as mediators for electrons transfer to the *4-NP* during the photoreduction process, as will be shown later in the text.

To evaluate the scavenging capability of the holes photogenerated when CdS/ITO films are illuminated with blue light, photocurrent vs potential curves were obtained using the same LED lamp employed for the photocatalysis tests, see Fig. 8b. The experiment started under illumination at 0.8 V, then the potential was scanned in the cathodic direction at a rate of 20 mVs^{-1} and the blue-light was simultaneously chopped. Low photocurrent was obtained in electrolyte labeled as support but the addition of sulfite and citric acid increases the measured photocurrent, indicating that sulfite and citric acid are effectively scavenging the photogenerated holes in the CdS photocatalysts. Additionally, the on-set of the photocurrents, i.e. the lower potential value at which anodic photocurrents are observed, is displaced towards more negative values in a similar way than the E_{fb} (see Table 1). So, sulfite ions and citric acid are playing a dual role during the photocatalytic process acting as hole-scavenger and displacing the reduction potential of the photogenerated electrons in CdS towards more negative values, offering a higher potential difference to perform the *4-NP* photocatalytic reduction.

Another way to track the trapping, accumulation and transferring of the photogenerated electrons in n-type semiconductors is by measuring the variations of the open circuit potential (OCP) under illumination, and its recovering when light is interrupted [45]. For these reason, the OCP was measured in the three different scenarios and two perturbations of 1 min were performed with blue-light in order to photoexcite the electrons to the conduction band of CdS; after that the recovery of the OCP was followed to detect the recombination or transfer of electrons to species in solution. Furthermore, as the potential observed is the same of the nanoparticles in suspension when the photocatalytic process is performed (no electrochemical bias is imposed), it is a more realistic approximation to what is taking place in suspension, compared to that observed from voltammetry measurements. For this reason, OCP measurements were also carried out in absence and presence of *4-NP*.

In all cases, the OCP versus time curves (Fig. 9) rapidly turned more negative when the CdS films were perturbed with blue-light, behavior characteristic of n-type semiconductors that evidence the accumulation of the photogenerated electrons on its conduction band. When sulfite (Fig. 9) and sulfite + citric acid (Fig. 9) were added, the OCP under

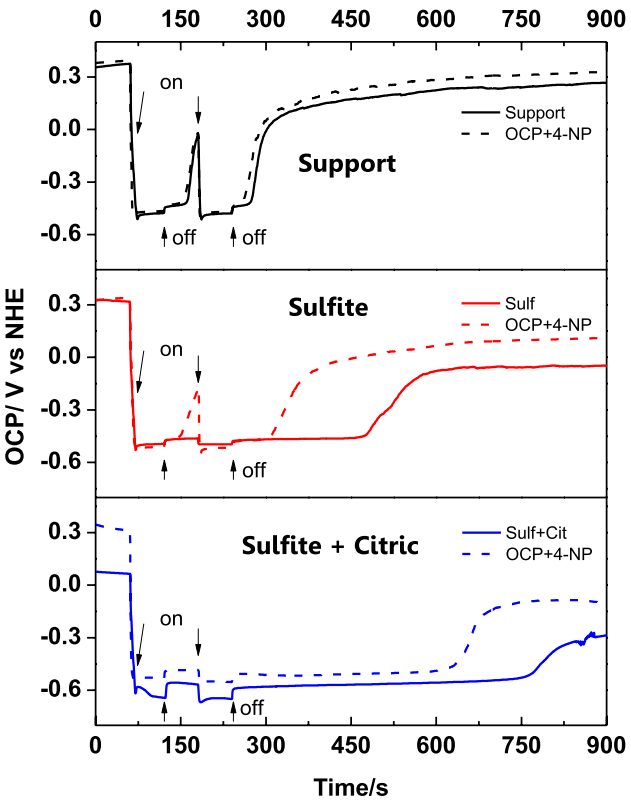

Fig. 9 Plot of OCP versus time curves obtained for the CdS/ITO in the three different scenarios in absence and presence of *4-NP*

illumination turned more negative (from −0.5 to −0.65 eV) which is in line with the variation in the E_{fb} (Table 1) and the photocurrent on-set (Fig. 8b). Additionally, the recovery of the OCP showed differences depending of the composition of the electrolyte. In the electrolyte labeled as support, the OCP showed a rapid decrement when the blue-light was definitively interrupted, followed by a potential plateau during a small period of time (40 s), indicating the presence of shallow energetic states under the conduction band of the CdS [46], and finally, the OCP decreased exponentially towards values similar to those obtained in the dark. When *4-NP* was added, the OCP vs time curve measured was just slightly modified, indicating that the photogenerated electrons are not transferred to *4-NP* in absence of sulfite ions.

Nonetheless, when sulfite ions were added to the electrolyte support the potential under illumination turned more negative than in absence of sulfite ions, and two big changes in the OCP recovering process can be detected (Fig. 9): *(i)* the potential plateau is maintained for a longer period of time (230 s) at a slightly more negative value than in the supporting electrolyte, indicating that a higher quantity of shallow energetic states were created due to the adsorption of SO_3^{2-} ions, and *(ii)* when this shallow energetic states are depleted, the OCP did not recover its dark-condition value; instead, it reaches a new plateau indicating the presence of deeper energetic states that traps the photogenerated electrons. Furthermore, when citric acid and sulfite ions were simultaneously added to the electrolyte (Fig. 9), the plateaus were detected at more negative potential values and for longer periods of time (510 s), indicating the generation of a larger quantity of shallow energetic states in the CdS. These changes in the population of energetic states correlate well with the changes in the semiconducting properties (Fig. 8). Finally, when *4-NP* was added to the electrolytes employed (sulfite and sulfite + citric), the OCP recovers in shorter periods of times, (70 and 360 s, respectively) indicating that *4-NP* is scavenging the photogenerated electrons accumulated in the different shallow energetic states. However, when the citric acid is added, the recovering time of the OCP is five times larger indicating that electrons trapped in these states do not recombine and are used for the electron transfer process during the *4-NP* photocatalytic reduction.

3.7 Mechanism of *4-NP* photoreduction using SO_3^{2-} ions

To establish the photocatalytic mechanism for the reduction of the *4-NP* to *4-AP* using either SO_3^{2-} or HSO_3^- ions on CdS nanofibers under blue light irradiation, several aspects should be taken into consideration:

1) In acid media at pH < 6, the *4-NP* (neutral) and HSO_3^- ions are the predominant species in the solution and the CdS is prone to be dissolved, but in alkaline media at pH > 8, the *4-NPhate* (anionic) and SO_3^{2-} ions are the predominant species in the solution and the CdS is chemically stable.
2) The photodecomposition of either SO_3^{2-} or HSO_3^- ions yield to the formation of $\bullet SO_3^-$ radical in the same way, acting as "hole scavenger". The redox potential of the couple $\bullet SO_3^-/SO_3^{2-}$ at pH 9 is within 0.6–0.9 eV [39, 47].
3) The position of the conduction band of CdS in the presence of SO_3^{2-} ions at pH ~ 9, is negative enough (−0.7 V vs. NHE), suggesting that photogenerated electrons can directly be transferred to *4-NP* in water [48].

Several investigations have suggested that the *4-NP* reduction reaction is dominated by the co-adsorption of *4-NPhate* and SO_3^{2-} ions to induce the electron transfer on semiconductor surfaces [49, 50]. However, it has been recently demonstrated that the adsorption of either *4-NPhate* or *4-NP* on semiconductor surface occurs via nitrogroup (–NO_2) [38]. Therefore, the blue-photogenerated *holes* (h^+) are consumed by either HSO_3^- or SO_3^{2-} ions adsorbed on CdS nanofibers surface, forming sulfite ($\bullet SO_3$) radicals that leads to the formation of sulphate (SO_4^{2-}) ions [17, 18], whereas the blue-photogenerated *electrons* (e^-) are transferred from shallow energetic states located under the conduction band of CdS to the adsorbed acceptor nitrogroup (*4-NPhate* or *4-NP)* to form aminophenol [25].

3.8 Mechanism of *4-NP* photoreduction using SO_3^{2-} ions and carboxylic acid

To establish the photocatalytic mechanism for *4-NP* reduction using either SO_3^{2-} or HSO_3^- ions in the presence of carboxylic acid on CdS nanofibers, new aspects should be considered:

1) The used carboxylic acids cannot acts as "hole scavenger" by using CdS nanofibers, because the blue-photogenerated *holes* hardly react with the carboxylic acid to form $\bullet CO_2^-$ radicals due to the low redox potential of the valence band of CdS [14].
2) The carboxylic acid can be linked to the superficial Cd^{2+} of the CdS, creating more shallow energetic states on CdS nanofibers, being chemically stable at pH 6–8 [40].

When different middle carboxylic acid are used in the *4-NP* photoreduction in the presence of SO_3^{2-} ions, they interact with CdS in different way (Fig. 10). Oxalic acid is hardly adsorbed on CdS surface and the *4-NP* photoreduction reaction rate is low, but either acetic or citric acid is well adsorbed on CdS surface and the "hole scavenging effect" by either

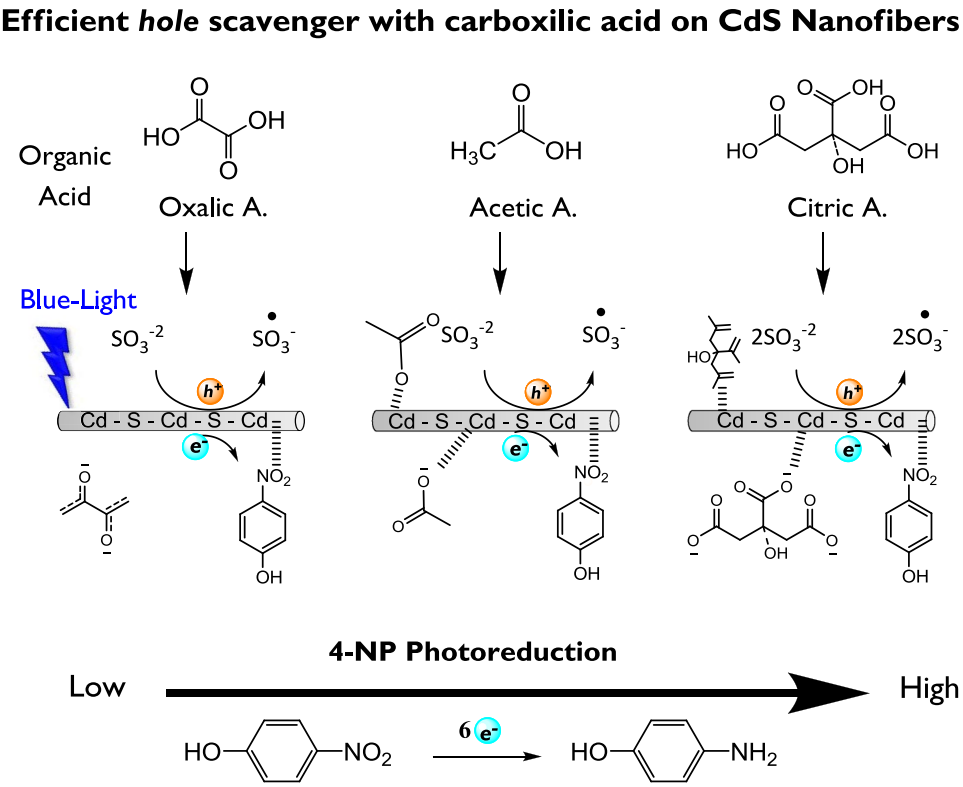

Fig. 10 Schematic of enhanced "hole scavenging effect" using Na_2SO_3 in the presence of middle carboxylic acid for the *4-NP* photoreduction

HSO_3^- or SO_3^{2-} ions is 3 or 5 times increased, respectively, and the 4-*NP* photoreduction reaction rate is high.

4 Conclusion

The *4-NP* photoreduction rate by using CdS nanofibers was successfully enhanced due to the *holes* consumption with either HSO_3^- or SO_3^{2-} ions in the presence of organic carboxylic acid. The fast electron transfer process strongly depends on the photocatalyst load, type of the carboxylic acid and its concentration (4 mM for citric acid). The highest *4-NP* photoreduction rate achieved with citric acid was associated to the capacity of adsorption on the CdS surface to create shallow energetic states under the conduction band of CdS to avoid the electron–hole recombination. CdS nanofibers can be recycled by four cycles with high chemical stability. The photoreduction of *4-NP* containing Na_2SO_3 and organic carboxylic acids under visible light can be achieved with great efficiency in the solar chemical conversion.

Acknowledgements The author thank to CONACYT for the Catedras-Conacyt/1169. The authors also acknowledge the financial support from UNAM-PAPIIT IN106015 project.

References

1. H.K. Kadam, S.G. Tilve, RSC Adv. **5**, 83391–83407 (2015)
2. S.H. Frank, A. Baron, N.J., assignor, United States Patent 0″ C6 (1972)
3. R. Ma, Y.-J. Kim, D.A. Reddy, T.K. Kim, Ceram. Int. **41**, 12432–12438 (2015)
4. Z. Zand, F. Kazemi, S. Hosseini, Tetrahedron Lett. **55**, 338–341 (2014)
5. H. Park, D.A. Reddy, Y. Kim, S. Lee, R. Ma, M. Lim, T.K. Kim, Appl. Surf. Sci. **401**, 314–322 (2017)
6. Y. Kim, R. Ma, D.A. Reddy, T.K. Kim, Appl. Surf. Sci. **357**, 2112–2120 (2015)
7. Y. Shiraishi, Y. Togawa, D. Tsukamoto, S. Tanaka, T. Hirai, ACS Catal. **2**, 2475–2481 (2012)
8. W. Wu, G. Liu, S. Liang, Y. Chen, L. Shen, H. Zheng, R. Yuan, Y. Hou, L. Wu, J. Catal. **290**, 13–17 (2012)
9. D. Guerrero-Araque, P. Acevedo-Peña, D. Ramírez-Ortega, R. Gómez, New J. Chem. **41**, 12655–12663 (2017)
10. J. Su, X.X. Zou, G.D. Li, L. Li, J. Zhao, J.S. Chen, Chem. Commun. (Camb) **48**, 9032–9034 (2012)
11. B. Pal, B. Pal, Chem. Eng. J. **263**, 200–208 (2015)
12. R.M. Mohamed, F.M. Ibrahim, J. Ind. Eng. Chem. **22**, 28–33 (2015)
13. P. Roy, A.P. Periasamy, C.T. Liang, H.T. Chang, Environ. Sci. Technol. **47**, 6688–6695 (2013)
14. W. Wu, G. Liu, Q. Xie, S. Liang, H. Zheng, R. Yuan, W. Su, L. Wu, Green Chem. **14**, 1705 (2012)
15. X. Pan, Y.-J. Xu, ACS Appl. Mater. Interfaces **6**, 1879–1886 (2014)
16. F.-X. Xiao, J. Miao, B. Liu, Mater. Horiz. **1**, 259–263 (2014)
17. A. Hernández-Gordillo, A.G. Romero, F. Tzompantzi, R. Gómez, Appl. Catal. B **144**, 507–513 (2014)
18. A. Hernández-Gordillo, A.G. Romero, F. Tzompantzi, S. Oros-Ruiz, R. Gómez, J. Photochem. Photobiol. A **257**, 44–49 (2013)

19. S. Ramírez-Rave, A. Hernández-Gordillo, H.A. Calderón, A. Galano, C. García-Mendoza, R. Gómez, New J. Chem. **39**, 2188–2194 (2015)
20. A. Hernández-Gordillo, S. Obregón, F. Paraguay-Delgado, V. Rodríguez-González, RSC Adv. **5**, 15194–15197 (2015)
21. P. Suyana, S.K. R, B.N. Nair, V. Karunakaran, A.P. Mohamed, K.G.K. Warrier, U.S. Hareesh, RSC Adv. **6**, 17800–17809 (2016)
22. C. Xu, Y. Yuan, R. Yuan, X. Fu, RSC Adv. **3**, 18002 (2013)
23. K. Imamura, S. Iwasaki, T. Maeda, K. Hashimoto, B. Ohtani, H. Kominami, Phys. Chem. Chem. Phys. **13**, 5114–5119 (2011)
24. P. Eskandari, F. Kazemi, Z. Zand, J. Photochem. Photobiol. A **274**, 7–12 (2014)
25. S. Liu, M.-Q. Yang, N. Zhang, Y.-J. Xu, J. Energy Chem. **23**, 145–155 (2014)
26. W. Wu, R. Lin, L. Shen, R. Liang, R. Yuan, L. Wu, Phys. Chem. Chem. Phys. **15**, 19422 (2013)
27. Z. Chen, S. Liu, M.Q. Yang, Y.J. Xu, ACS Appl. Mater. Interfaces **5**, 4309–4319 (2013)
28. S.K. Pahari, P. Pal, D.N. Srivastava, S. Ghosh, A.B. Panda, Chem. Commun. (Camb) **51**, 10322–10325 (2015)
29. A. Hernández-Gordillo, A.G. Romero, F. Tzompantzi, R. Gómez, Powder Technol. **250**, 97–102 (2013)
30. P.W. Ursula, Deister, J. Phys. Chem. **94**, 2191–2198 (1990)
31. B. Podkrajšek, I. Grgić, J. Turšič, G. Berčič, J. Atmos. Chem. **54**, 103–120 (2006)
32. A. Hernandez-Gordillo, S. Oros-Ruiz, R. Gomez, J Coll. Interface Sci. **451**, 40–45 (2015)
33. M. Tang, G. Huang, S. Zhang, Y. Liu, X. Li, X. Wang, X. Pang, H. Qiu, Mater. Chem. Phys. **145**, 418–424 (2014)
34. P. Dauthal, M. Mukhopadhyay, Indus. Eng. Chem. Res. **51**, 13014–13020 (2012)
35. A.I. Biggs, Trans. Faraday Soc. **50**, 800–802 (1954)
36. P.W. Michael Fischer, J. Phys. Chem. **100**, 15111–15117 (1996)
37. A.T.E. Hayon, J. Wilf, J. Am. Chem. Soc. **94**, 47–57 (1971)
38. M. Muniz-Miranda, Appl. Catal. B **146**, 147–150 (2014)
39. C.B.a.R.v. Eldi, Chem. Rev. **95** 119–190 (1995)
40. R.F. Domingos, C. Franco, J.P. Pinheiro, Environ. Sci. Pollut. Res. Int. **20**, 4872–4880 (2013)
41. T. Simon, N. Bouchonville, M.J. Berr, A. Vaneski, A. Adrovic, D. Volbers, R. Wyrwich, M. Doblinger, A.S. Susha, A.L. Rogach, F. Jackel, J.K. Stolarczyk, J. Feldmann, Nat. Mater. **13**, 1013–1018 (2014)
42. M. El-rouby, A.S. Aliyev, J. Mater. Sci.: Mater. Electron. **25**, 5618–5629 (2014)
43. A. Salabat, F. Mirhoseini, Photochem. Photobiol. Sci. **14**, 1637–1643 (2015)
44. M.B.-Z. Maria del Mar Cordero-Rando, J.M. BarberaÂ-Salvador, I. Naranjo-Rodríguez, J.A. Muñoz-Leyva, J.L. Hidalgo-Hidalgo de Cisneros, Mikrochim. Acta **132**, 7–11 (1999)
45. D. Ramírez-Ortega, A.M. Meléndez, P. Acevedo-Peña, I. González, R. Arroyo, Electrochim. Acta **140**, 541–549 (2014)
46. S. Li, L. Zhang, T. Jiang, L. Chen, Y. Lin, D. Wang, T. Xie, Chemistry **20**, 311–316 (2014)
47. P.N. Robert, E. Huie, J. Phys. Chem. **88**, 5665–5669 (1984)
48. P. warman, J. Phys. Chem. Ref. Data **18**, 1637–1755 (1989)
49. Y. Su, X. Xin, Y. Wang, T. Wang, X. Wang, Chem. Commun. (Camb) **50**, 4200–4202 (2014)
50. M. Liu, L. Lv, X. Du, J. Lang, Y. Su, Y. Zhao, X. Wang, RSC Adv. **5**, 103013–103018 (2015)